

High-efficiency wide-angle anomalous refraction with acoustic metagrating

Kangyao Sun(孙康瑶), Yuancheng Fan(樊元成), Zhehao Ye(叶哲浩), Jiahui Li(李嘉荟), Quanhong Fu(付全红), Yali Zeng(曾雅丽), and Fuli Zhang(张富利)

Citation: Chin. Phys. B, 2025, 34 (**1**): 014302. DOI: 10.1088/1674-1056/ad8db6
Journal homepage: http://cpb.iphy.ac.cn; http://iopscience.iop.org/cpb

What follows is a list of articles you may be interested in

One-dimensional $\mathcal{PT}$ -symmetric acoustic heterostructure

Hai-Xiao Zhang(张海啸), Wei Xiong(熊威), Ying Cheng(程营), and Xiao-Jun Liu(刘晓峻)
Chin. Phys. B, 2022, 31 (**12**): 124301. DOI: 10.1088/1674-1056/ac90b3

Three-dimensional coupled-mode model and characteristics of low-frequency sound propagation in ocean waveguide with seamount topography

Ya-Xiao Mo(莫亚枭), Chao-Jin Zhang(张朝金), Li-Cheng Lu(鹿力成), and Sheng-Ming Guo(郭圣明)
Chin. Phys. B, 2022, 31 (**8**): 084301. DOI: 10.1088/1674-1056/ac538f

Frequency-dependent reflection of elastic wave from thin bed in porous media

Hong-Xing Li(李红星), Chun-Hui Tao(陶春辉), Cai Liu(刘财), Guang-Nan Huang(黄光南), Zhen-An Yao(姚振岸)
Chin. Phys. B, 2020, 29 (**6**): 064301. DOI: 10.1088/1674-1056/ab888b

Simulation of acoustic fields emitted by ultrasonic phased array in austenitic steel weld

Zhong-Cun Guo(郭忠存), Shou-Guo Yan(阎守国), Bi-Xing Zhang(张碧星)
Chin. Phys. B, 2019, 28 (**11**): 114302. DOI: 10.1088/1674-1056/ab4d41

A three-dimensional coupled-mode model for the acoustic field in a two-dimensional waveguide with perfectly reflecting boundaries

Wen-Yu Luo(骆文于), Xiao-Lin Yu(于晓林), Xue-Feng Yang(杨雪峰), Ze-Zhong Zhang(张泽众), Ren-He Zhang(张仁和)
Chin. Phys. B, 2016, 25 (**12**): 124309. DOI: 10.1088/1674-1056/25/12/124309

High-efficiency wide-angle anomalous refraction with acoustic metagrating

Kangyao Sun(孙康瑶), Yuancheng Fan(樊元成)†, Zhehao Ye(叶哲浩), Jiahui Li(李嘉荟), Quanhong Fu(付全红), Yali Zeng(曾雅丽), and Fuli Zhang(张富利)‡

MOE Key Laboratory of Material Physics and Chemistry under Extraordinary Conditions, School of Physical Science and Technology, Northwestern Polytechnical University, Xi'an 710129, *China*

(Received 30 September 2024; revised manuscript received 28 October 2024; accepted manuscript online 1 November 2024)

The emergent metagrating, with its unique and flexible beam shaping capabilities, offers new paths to efficient modulation of acoustic waves. In this work, an acoustic metagrating is demonstrated for high-efficiency and wide-angle anomalous refraction. It is shown that the normal reflection and transmission can be totally suppressed by properly modulating the amplitude and phase characteristics of the metagrating supercells for high-efficiency anomalous refraction. The anomalous refraction behavior is achieved in the wide range of incident angles from 28° to 78°, and the efficiency of −1st order diffraction is higher than 90% by finely designing the metagrating structure. The anomalous refraction behaviors are verified experimentally at incidence angle of 28°, 45°, and 78°, respectively. The demonstrated metagrating is anticipated to possess efficient wide-angle composite wavefront engineering applications in such fields as communications.

Keywords: acoustic metagrating, beam steering, wide-angle anomalous refraction

PACS: 43.20.El, 43.40.+s, 81.05.Xj

DOI: 10.1088/1674-1056/ad8db6 **CSTR:** 32038.14.CPB.ad8db6

1. Introduction

Metasurface have been demonstrated with efficient and flexible beam modulation properties.[1–3] The phase gradient metasurface has grown rapidly and gained widespread attention in both physics and engineering, opening the way for complex wavefront control in acoustics.[4–9] Various functional acoustic devices with excellent performance can be designed by properly designing the structure, size, and other parameters.[10–19] Recently, applications based on transmissive metasurface, such as high numerical aperture, large angle steering, and device miniaturization, have gained extensive attention.[20–22] However, due to the beam modulation method generally relies on local resonance or scattering modes of independent units and the output energy evaporates as the angle of incidence approaches a critical angle, traditional phase gradient metasurface often suffers from low spatial frequency and diffraction efficiency.[23–25]

Many approaches to improve the efficiency of anomalous refraction for transmissive metasurfaces have been successively reported.[26,27] For example, the efficiency of wide-angle beam deflection can be improved by using bianisotropy metasurfaces.[28] Recently, metagrating has been proposed and demonstrated as another type of artificial planar structures that overcomes the fundamental limitation of the critical incident angles for the phase gradient method.[29–33] Combination of the advantages of metasurface and traditional grating, acoustic energy direction is manipulated in a single availably, suppresses normal order output waves due to the synergy effect between acoustic diffraction and phase modulation. Several design strategies for metagrating device have been reported at present.[31,34–38] Xu *et al*. designed an acoustic phase gradient metagratings composed of periodic supercells and revealing its diffraction mechanism.[39] Zhang investigated the theoretical extension of two-dimensional (2D) metagratings to manipulate waves in three-dimensional (3D) spaces, adding an extra dimension to modern holographic design and metasurface wavefront manipulation.[40] However, previous researches have mainly focused on the anomalous refraction of specific incident waves, which is unable to meet the requirements of practical wide-angle applications.

In this paper, high-efficiency and wide-angle anomalous refraction has been achieved through coherently modulating different order components of the transmitted acoustic field. By adjusting the geometric parameters of the unit to suppress the higher order, the interference phase eliminates the normal order and retains only the −1st order component to realize the abnormal refraction function. The transmission phase difference of units A and B varies linearly over a wide range of incidence angles at operating frequency, enabling the metagating to perform effectively at various incidence angles with efficiency higher than 90%. Simulation and experiment indicate the designed acoustic metagrating device achieve beam steering at the wide incident angle ranges of 28°–78°.

†Corresponding author. E-mail: phyfan@nwpu.edu.cn

‡Corresponding author. E-mail: fuli.zhang@nwpu.edu.cn

© 2025 Chinese Physical Society and IOP Publishing Ltd. All rights, including for text and data mining, AI training, and similar technologies, are reserved.

2. Design and results

If the grating constant (p) is equal to or smaller than the wavelength of the acoustic wavelength, one or more diffraction orders can be produced when the obliquely incident acoustic wave at angle θ_{in} passes through the transmission-type acoustic metagrating device. The diffraction angle for various diffraction orders have been calculated by diffraction formula, denoted as $p(n_2 \sin\theta_{tr} - n_1 \sin\theta_{in}) = m\lambda_0$, where n_1 and n_2 are the refractive indices of the medium at the upper and lower of the acoustic metagrating, respectively, both of which are 1 here. And θ_{tr} is the refractive angle, λ_0 is the wavelength, and m is the diffraction order. The scattering properties of the metagrating are been altered to obtain the desired diffraction order by adjusting the length of each period. Therefore, for obliquely incident acoustic waves, if the diffraction wave only exists in the highest order of the $\pm$1st order diffraction wave, it needs to meet $p < \frac{2\lambda_0}{|\sin\theta_{in}|+1}$. Furthermore, in the case of oblique incidence, if $p < \frac{\lambda_0}{1-|\sin\theta_{in}|}$ is satisfied, there is no $+1$st order sound wave in the transmitted field. Under oblique incidence, if the wavelength and period satisfy the above equation, the system will exhibit normal and -1st order diffraction. By eliminating the normal order diffracted waves, it is possible to achieve efficient transmission of sound waves in the direction of the -1st order diffraction. When the phase difference between adjacent units is π within a period, interference elimination occurs after the acoustic wave passes through the metagrating, and the normal order diffraction wave is suppressed.

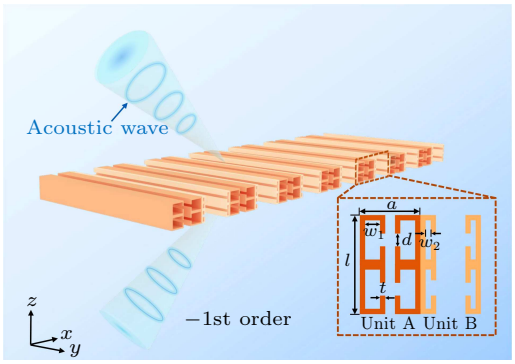


Fig. 1. Schematic diagram of the metagrating of the modulated acoustic wave showing anomalous refraction under oblique incidence, and the inset shows the sketch of the unit cell, which consists of units A and B with periodic $p = 2a$.

The metagrating consists of two units (A and B) in a periodic with the height of l, a 2D structure invariant along the y direction, as shown in Fig. 1. Two side-open symmetrically juxtaposed Helmholtz cavities being got for each unit utilize to provide sufficient phase modulation. And the volume of the Helmholtz resonance cavities of units A and B can be adjusted by varying the parameter w, as they have different volumes. The width of each unit is $a = p/2 = 60$ mm, the opening width of each air cavity is $d = 4$ mm, the thickness of the side wall is $t = 2$ mm, and the height of the whole structure is $l = 38$ mm respectively. In this work, 2020 Hz is chosen as the operating frequency. COMSOL Multiphysics software was used to simulate the calculations with an air density of 1.21 kg/m^3 and a sound velocity of 343 m/s. The incident acoustic wave is set as a plane wave with an amplitude of 1 Pa, and periodic boundaries are applied on both sides of the structure to simulate an infinite row of units. The perfectly matched layers are used to attenuate the field of outward radiation without reflection.

When the grating constant p is determined, the operating wavelength only needs to be slightly larger than p ($< \lambda_0$), in this way, $\frac{p}{\lambda_0} < 1 < \frac{2}{|\sin\theta_{in}|+1}$ and $\frac{p}{\lambda_0} < 1 < \frac{1}{1-|\sin\theta_{in}|}$ are satisfied for any angle oblique incident acoustic wave. At this point, only the -1st and normal order diffraction waves are presented in the transmitted field. It is essential to maximize the reduction of normal order diffraction by adjusting the phase of the unit to achieve abnormal refraction. We have selected an operating frequency of 2020 Hz, $\theta_{in} = 45°$, corresponding to a wavelength that fulfills the constraints. The phase and transmission coefficients of individual structural units change as w varies from 2 mm to 25 mm as shown in Fig. 2(a). It is evident that the coverage during the transmission phase exceeds π, and it is always possible to locate two units with a phase difference of π. Transmittance is a crucial factor that must be taken into account for transmissive metasurfaces. We initially chose unit A with $w_1 = 19.1$ mm, corresponding to a transmittance and phase of 0.99 and 1.49 rad, respectively. In addition, we can always look for unit B with its phase difference of π and higher transmission coefficient, i.e., $w_2 = 3$ mm. Both points correspond to higher transmission values, and the phase difference complies with our design philosophy.

The two units periodically align to construct the metagrating. The normalized diffraction orders in the transmitted acoustic field are calculated, as shown in Fig. 2(b). It is observed that the normal order diffraction is near 0 at the operating frequency $f_1 = 2020$ Hz, while -1st order diffraction close to 100%. At the same time, the metagrating has a high transmittance at the operating frequency. The scattered acoustic field distribution of the metagrating is demonstrated as in Figs. 2(c)–2(e). At the operating frequency, the abnormal refraction is obvious when the acoustic wave is oblique incident at 45°. The transmitted wave propagates along the direction of the -1st order diffraction angle, and the diffraction angle $\theta_{tr} = -45°$ obtained by simulation agrees with the theoretical value calculated by the diffraction formula. The non-operating frequency $f_2 = 2200$ Hz was chosen as a comparison, and the anomalous transmission phenomenon was not observed from the transmission field in Fig. 2(e). At this frequency point, the diffraction efficiencies of the -1st and normal orders account for the same percentage, and the standing waves are formed by two types diffracted waves in the transmitted field.

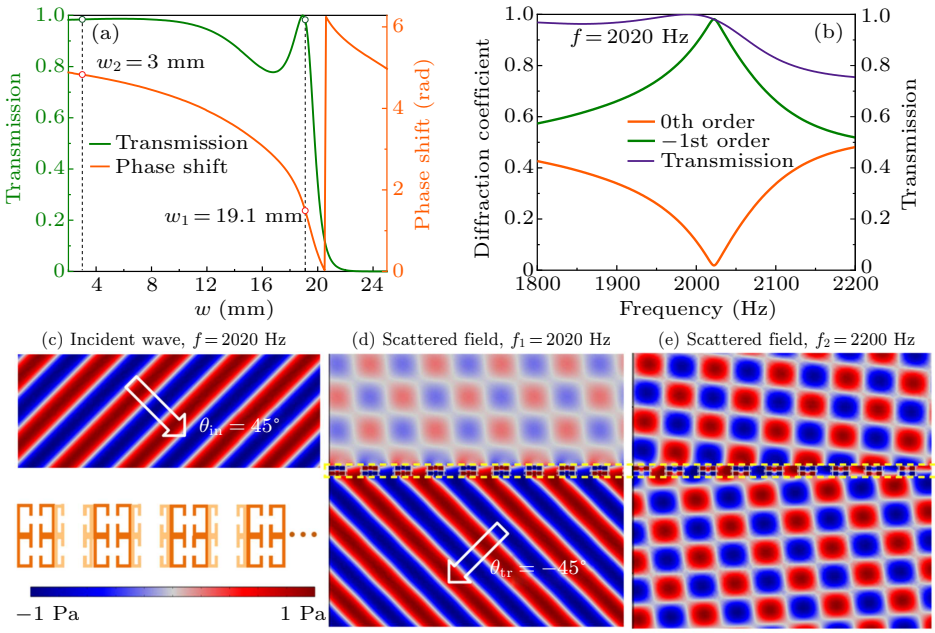


Fig. 2. Behaviour of metagrating modulated acoustic waves. (a) The phase shifts and transmission coefficient induced by single unit as a function of w, at $f = 2020$ Hz. (b) The normalized coefficients of each diffraction order in the transmission fields. Green and orange lines represent −1st and normal order diffraction, respectively. Purple line represents the transmission coefficient at different frequencies. (c) Incident acoustic fields with plane wave (upper) and the enlarged diagram of the proposed metagrating (bottom). (d) Scattered pressure fields at working frequency $f_1 = 2020$ Hz. (e) Transmitted pressure fields at non-working frequency $f_2 = 2200$ Hz.

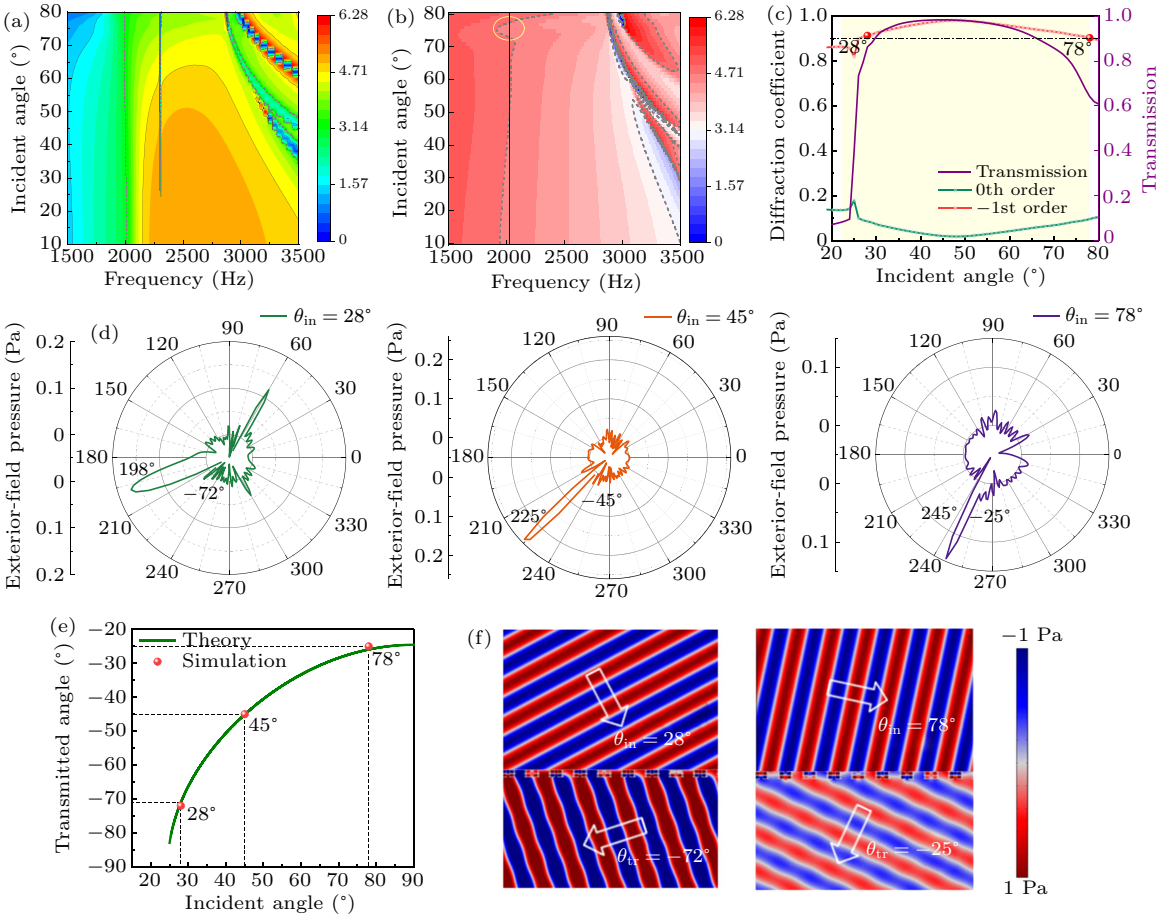


Fig. 3. Metagrating achieve anomalous transmission modulation at different incidence angles. (a) Transmission phase difference between units A and B varies with frequency and incident angle. (b) Transmission phase varies with frequency and incident angle when operating as a single unit. (c) Normalized −1st (red curves) and normal order (green curves) diffraction coefficients at 2020 Hz under different incident angles in the transmission fields. Transmittance curves (purple) at 2020 Hz under different incident angles. (d) The exterior-field pressure under different incident angles at the operating frequency of 2020 Hz. (e) Relationship between incident angle and transmission angle. (f) Incident acoustic fields and transmitted acoustic fields under the incident angles of 28° and 78°.

The modulation behavior of the designed metagrating for various incidence angles has been investigated simultaneously in our work. Figure 3(a) shows the variation of the transmission phase difference between units A and B as a function of frequency and incidence angle, whereas the gray dotted line near the operating frequency 2020 Hz indicates a phase difference of π. The change for the transmission phase difference between units A and B is not significant over the incidence angle of 10°–80°, indicating that the metagrating can effectively operate over a wide range of angles. However, transmission phase varies with frequency and incident angle when operating as a single unit as showed in Fig. 3(b), the transmission phase abruptly changes at an incident angle of near 78°, resulting in the incident beam not being modulated efficiently. The relationship between the normalized diffraction coefficients of normal and −1st order with the incident angle is numerically calculated, as shown in Fig. 3(c). In Fig. 3(c), the yellow area refers to the range of incidence angles where the −1st order diffraction in the transmitted field exceeds 90%. Moreover, it can be observed that the designed metagrating maintains a high transmittance within this region. In Fig. 3(d), the exterior-field pressure of the metagrating is depicted at incident angles of 28°, 45°, and 78°. The sound waves incident at various angles propagate in the direction of the −1st order after passing through the metagrating. The calculated diffraction angles of the −1st order are −72°, −45°, and −25°, respectively. Figure 3(e) shows the relationship between the incident angle and transmitted angle, in which the simulated result (red dot) is in good agreement with the theoretical value (green solid line) calculated by the diffraction formula. Numerical simulations of the acoustic pressure distributions in the region with high diffraction efficiency for the incident angles of 28° and 78° are shown in Fig. 3(f). Excellent abnormal refraction phenomenon could be observed in the transmitted field, where the transmitted waves propagate along the −1st order diffraction angle direction, and is consistent with the theoretical value calculated by the diffraction equation. In summary, it is verified in the simulation that the proposed metagrating has the abnormal refraction characteristic of wide angle (28°–78°) incidence.

The anomalous diffraction behavior of the designed metagrating composed of units A and B, operating at wide angles, is experimentally confirmed. The schematic diagram of the experimental test system for the 2D acoustic pressure field scanning platform is depicted in Fig. 4(a), with a computer controlling the entire scanning platform for sound generation, acquisition, and movement. Eight equidistant loudspeakers are positioned at the front of the waveguide as the sound source signal. The 2D waveguide is consisted by two acrylic plates placed parallel to each other with length, width, and thickness of 2.2 m, 1.2 m, and 0.02 m, respectively. The distance between the two parallel plates is 6 cm, and the 2020-Hz acoustic wave can be considered as a full-wave experiment when transmitted in the waveguide according to the acoustic wave transmission condition. The material density is 1200 kg/m^3, which is much higher than the density of air. To reduce the influence of other noises on the experiment, a lot of sound absorbing foams are placed around the waveguide. The sample is prepared by means of 3D printing technology and the polymer material (PLA, 1250 kg/m^3) is considered as the printing material, as illustrated in the inset of Fig. 4(a).

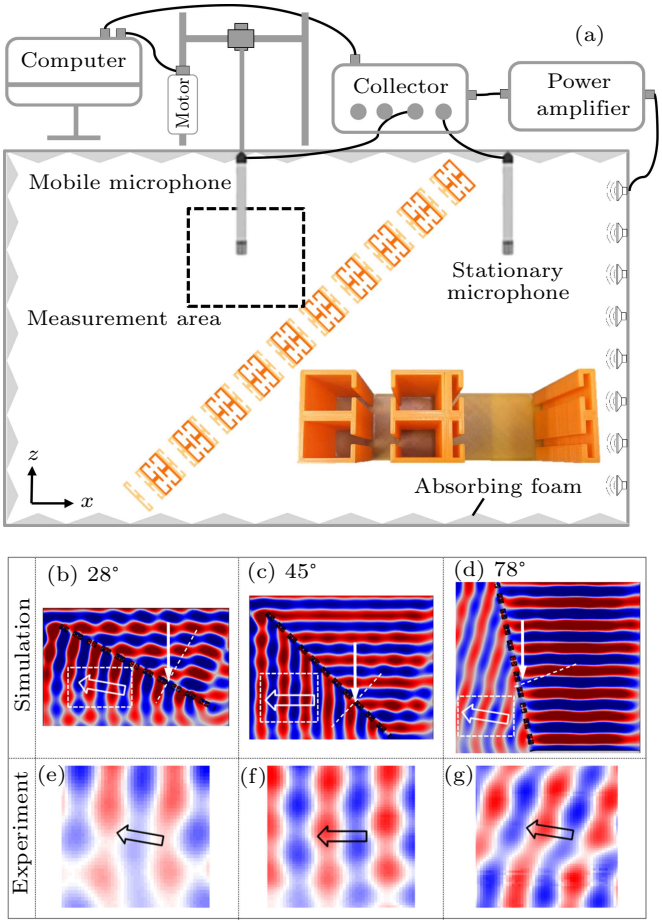


Fig. 4. Experimental verification of anomalous transmission behavior at various incidence angles. (a) Schematic representation of the experimental setup. The black dashed line box represents the measurement area where a mobile microphone is used to scan and measure acoustic pressure. The illustration is physical image of the samples in one acoustic grating period. (b)–(d) Simulated acoustic pressure fields under actual conditions of 28°, 45°, and 78°. (e)–(g) The experimental transmitted acoustic pressure fields of plane acoustic wave passing through the sample under different incident angles.

Due to the fixed position of the loudspeaker array, the samples need to be placed at 28°, 45°, and 78° to the z-axis to verify the anomalous transmission phenomenon. And the 11 periods of simples can be arranged owing to the limitation of the size of the waveguide. The acoustic pressure field distribution at different angles of incidence has been recalculated to more realistically simulate the experimental environment, as illustrated in Figs. 4(b)–4(d). The solid arrows show the direction of incident wave and the white box represents the experimental measurement area. The field distributions measured at

different incidence angles are shown in Figs. 4(e)–4(g), where the black hollow arrows depict their transmission directions, agreeing well with the simulation corresponding to the white dashed box. After the obliquely incident acoustic wave passes through the designed acoustic metagrating, the −1st diffracted wave dominates in the transmitted field, and the anomalous refraction phenomenon is realized. The proposed metagrating proved to be effective in adjusting the beam deflection over a wide range of incidence angles.

3. Conclusion

In this paper, a transmissive metagrating, utilizing the Helmholtz resonant cavity, effectively is proposed to realize anomalous refraction over a wide range of incidence angles. The proposed mategrating device contains two units per period, significantly alleviating the designed complexity. By suppressing the higher order component and eliminating the normal order between the units, the transmitted field only retains the −1st order wave to achieve the abnormal refraction. Due to the insensitivity of the transmission properties of the unit structure to the angle, the proposed metagrating can work efficiently at different incidence angles with −1st order diffraction efficiency higher than 90%. The efficiently anomalous acoustic wave transmission behavior in the incidence ranges of 28°–78° have been confirmed by both simulation and experiment. The reported device is promising for high-efficiently and wide-angle complex wavefront engineering in high numerical aperture, large angle steering, and device miniaturization.

Acknowledgements

Project supported by the National Key Research and Development Program of China (Grant Nos. 2023YFB3811400 and 2022YFB3806000), the National Natural Science Foundation of China (Grant No. 12074314), the Science and Technology New Star Program of Shaanxi Province, China (Grant No. 2023KJXX-148), and the Fundamental Research Funds for the Central Universities.

References

[1] Yu N, Genevet P, Kats M A, Aieta F, Tetienne J, Capasso F and Gaburro Z 2011 *Science* **334** 333
[2] Wen Y and Zhou J 2019 *Mater. Today* **23** 37
[3] Assouar B, Liang B, Wu Y, Li Y, Cheng J and Jing Y 2018 *Nat. Rev. Mater.* **3** 460
[4] Tian Z, Shen C, Li J, Reit E, Gu Y, Fu H, Cummer S A and Huang T J 2019 *Adv. Funct. Mater.* **29** 1808489
[5] Quan L and Alù A 2019 *Phys. Rev. Lett.* **123** 244303
[6] Zhu Y F, Fan X D, Liang B, Cheng J C and Jing Y 2017 *Phys. Rev. X* **7** 021034
[7] Gerard N J R K, Cui H, Shen C, Xie Y, Cummer S, Zheng X and Jing Y 2019 *Appl. Phys. Lett.* **114** 231902
[8] Sun K, Zhang F, Chen S, Fu Q, Zeng Y and Fan Y 2024 *iScience* **27** 110504
[9] Zhou H, Fu W, Wang Y, Wang Y, Laude V and Zhang C 2021 *Mater. Des.* **199** 109414
[10] Tian Y, Wei Q, Cheng Y and Liu X 2017 *Appl. Phys. Lett.* **110** 191901
[11] Mei J, Ma G C, Yang M, Yang Z Y, Wen W J and Sheng P 2012 *Nat. Commun.* **3** 756
[12] Han C, Fan S, Li C, Chen L Q, Yang T and Qiu C W 2024 *Adv. Mater.* **36** 2311350
[13] Zhou M Q, Li Z X, Li Y, Wang Y C, Zhang J, Chen D D, Quan Y, Yang Y T and Fei C L 2024 *Chin. Phys. B* **33** 014303
[14] He J, Yu S, Jiang X and Ta D 2024 *Chin. Phys. B* **33** 054301
[15] Huang S, Zhou Z, Li D, Liu T, Wang X, Zhu J and Li Y 2020 *Sci. Bull.* **65** 373
[16] Wang W, Tan Y, Liang B, Ma G, Wang S and Cheng J 2021 *Phys. Rev. B* **104** 174301
[17] Zhang H, Wang Q, Fink M and Ma G 2024 *Nat. Commun.* **15** 1270
[18] Qi H B, Fan S W, Jiang M, Tang X L and Wang Y S 2024 *Extrem. Mech. Lett.* **67** 102120
[19] Zhao J, Li B W, Chen Z and Qiu C 2013 *Appl. Phys. Lett.* **103** 151604
[20] Zhou Y, Mao C, Gershnabel E, Chen M and Fan J A 2024 *Laser Photon. Rev.* **18** 2300988
[21] Liu W, Li Z, Cheng H, Tang C, Li J, Zhang S, Chen S and Tian J 2018 *Adv. Mater.* **30** 1706368
[22] Ren J and Hou Z 2024 *Phys. Rev. Appl.* **22** 014040
[23] Tang S, Ren B, Feng Y, Song J and Jiang Y 2021 *Appl. Phys. Lett.* **119** 071907
[24] Estakhri N M and Alù A 2016 *Phys. Rev. X* **6** 041008
[25] Díaz-Rubio A and Tretyakov S A 2017 *Phys. Rev. B* **96** 125409
[26] Sieck C F, Alù A and Haberman M R 2017 *Phys. Rev. B* **96** 104303
[27] Muhlestein M B, Sieck C F, Wilson P S and Haberman M R 2017 *Nat. Commun.* **8** 15625
[28] Li J, Shen C, Díaz-Rubio A, Tretyakov S A and Cummer S A 2018 *Nat. Commun.* **9** 1342
[29] Neder V, Ra'di Y, Alù A and Polman A 2019 *ACS Photon.* **6** 1010
[30] Ra'di Y and Alù A 2018 *ACS Photon.* **5** 1779
[31] Qian J, Xia J P, Sun H X, Wang Y, Ge Y, Yuan S Q, Yang Y H, Liu X J and Zhang B L 2020 *Adv. Mater. Technol.* **5** 2000542
[32] Cao J, Ma H, Xie S, Li J, Li Y and Cheng Q 2024 *Phys. Rev. Appl.* **21** 034015
[33] Tan Z, Yi J, Ratni B and Burokur S N 2024 *Phys. Rev. Appl.* **21** 024009
[34] Wang Y H, Cheng Y and Liu X J 2019 *Sci. Rep.* **9** 7271
[35] Song A, Sun C, Xiang Y and Xuan F Z 2022 *Appl. Phys. Express* **15** 024002
[36] Fu Y Y, Cao Y Y and Xu Y D 2019 *Appl. Phys. Lett.* **114** 053502
[37] Jin Y, Fang X, Li Y and Torrent D 2019 *Phys. Rev. Appl.* **11** 011004
[38] Quan J, Sun B, Fu Y, Gao L and Xu Y 2024 *Chin. Phys. Lett.* **41** 014301
[39] Fu Y Y, Shen C, Cao Y Y, Gao L, Chen H Y, Chan C T, Cummer S A and Xu Y D 2019 *Nat. Commun.* **10** 2326
[40] Zou H Y, Ge Y, Zhao K Q, Lu Y J, Si Q R, Yuan S Q, Chen H, Sun H X, Yang Y and Zhang B 2024 *Adv. Mater.* **36** 2401738